Chemical Methodologies

Journal homepage: http://chemmethod.com

Original Research Article

Cytotoxicity and Anticancer Effect of Chitosan-Ag NPs-Doxorubicin-Folic Acid Conjugate on Lungs Cell Line

Manar S. Jabar*, Shatha Abdul Wadood AL- Shammaree

Department of Chemistry, College of Science, University of Baghdad, Iraq

ARTICLE INFO

Article history

Submitted: 2022-06-30
Revised: 2022-08-21
Accepted: 2022-09-24
Manuscript ID: CHEMM-2208-1604
Checked for Plagiarism: Yes
Language Editor:
Dr. Fatimah Ramezani
Editor who approved publication:
Dr. Sami Sajjadifar

DOI:10.22034/CHEMM.2023.359769.1604

KEYWORDS

Chitosan
Doxorubicin
Silver nanoparticles
Folic acid
Lung cancer cell line A549

ABSTRACT

This study looked at how the synthetic chitosan-AgNPs-Doxorubicin-folic acid combination affected the A549 cell line in terms of cytotoxicity and anticancer activity. By reducing silver nitrate ($AgNO_3$) and biodegradable chitosan, silver nanoparticles were biosynthesized. The produced conjugate was examined by using FT-IR spectroscopy, atomic force microscopy (AFM), and field emission scanning electron microscopy (FE-SEM). The cytotoxicity assay for the viability of A549 cells revealed that the combination of chitosan, AgNPs, doxorubicin, and folic acid decrease cell viability in a dose-determined bymethod over 48 hours, which direct to a dependent reduce in the activity of A549 cells. The mechanism analysis of the impacted living cells leading to apoptosis revealed a considerable rise in nuclear concentration, cytochrome c, and cell membrane permeability (dose-dependent). The bright green chromatin in DOX-treated cells was compacted or broken up, indicating an early stage of apoptosis. However, cells treated with the CS-AgNPs-DOX-FA compound displayed orange nuclei and late stage apoptosis. The findings demonstrated that A549 lung cancer cells are cytotoxic to Cs-Ag NPs-DOX-FA. The Cs-Ag NPs-DOX-FA MTT assay demonstrated that the harmful effect of 25 µg/mL on A549 cells is dose-dependent, and a rise in nuclear intensity, membrane permeability, and cytochrome were observed. Cell viability also declined, and the potential of the mitochondrial membrane changed. The fact that the release of DOX was delayed shows that nanoparticles in drug carriers may be used to reduce the exposure of healthy tissues; however, boosting the accumulation to therapeutic medicine in the tumour site.

GRAPHICAL ABSTRACT

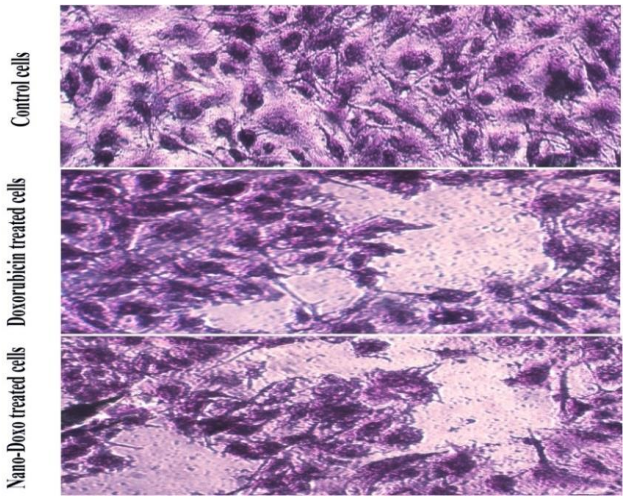

* Corresponding author: Manar S. Jabar
✉ E-mail: manolamanola2468@gmail.com

Introduction

Worldwide, cancer continues to be a serious illness with a high fatality rate. More than 31,500 cases of cancer and tumor-associated illnesses were reported in 2017–2018, according to data just made public by Iraq's National Cancer Registry. Locally, it is believed that cancer, which accounts for around 11% of the overall rate, is one of the central causes of death-rate [1].

The use of traditional chemical drugs has been linked to a growing number of restrictions, including their low specificity, erratic distribution in organs and tissues, and quick clearance [2]. This field of study applies nanotechnology while offering cutting-edge approaches for the treatment of numerous human ailments, including cancer [3].

The majority of nanomaterials possess special qualities making them useful in a range of biotechnological applications, which has led to their use in the creation of incredibly powerful diagnostic and therapeutic tools [4-6]. In addition, nanomaterials might be used in drug transmission systems to decline the adverse effects frequently connected with the usage of conventional pharmaceuticals [7, 8]. In the near future, it is anticipated that the food and drug administration (FDA) would approve an increasing number of these materials [9, 10]. Doxorubicin (DOX) has potent anticancer activities; however, the only factor that has been proven to increase the risk of DOX-mediated cardiotoxicity is the cumulative dosing. The therapeutic use of DOX is also hampered by drug-induced cancer resistance [3]. A modern approach to overcoming resistance is the use of two or more chemotherapeutics [4]. Even while such combination chemotherapies have a synergistic impact, clinical studies have demonstrated that their pharmacokinetic interactions have serious systemic side influence, like cardiotoxicity and bone marrow suppression [4-6]. Therefore, the creation of cutting-edge cancer treatment solutions is urgently needed. One method is to alter a well-researched chemotherapeutic medication, such as DOX, that would ideally have the following characteristics: selectively target and kill cancer cells, amended efficacy/toxicity impartiality, enhanced therapeutic index, and improved pharmacokinetics outline.

Designing a combination of chitosan, silver nanoparticles, doxorubicin, and folic acid (CS-AgNPs-DOX-FA) with the intention of improving anticancer drug delivery for lung cancer is the goal of this study.

Materials Methods

The materials and reagents utilized in this research are as follow: Chitosan (Ch) (Biomedical; India), Acetic acid (Sigma-Aldrich, USA), Silver nitrate ($AgNO_3$) (Sigma-Aldrich, USA), Sodium hydroxide (NaOH) (Spctrum; USA.), Acridine Orange–Ethidium Bromide Dual Staining (Sigma; Germany), Fluorescein Isothiocyanate Isomer I (Bio Basic; Canda), Trypsin (Golden Era Pharma; Mumbai), lung cancer cell line (A549), MTT, Folic acid, and RPMI-1640 Media were provided by Sigma-Aldrich (Germany).

Composition of chitosan-silver nanoparticles (CS-AgNPs)

A typical silver nanoparticle synthesis involved dissolving 1 g of chitosan in 5% CH_3COOH and stirring the mixture for thirty minutes. The solution was then filtered to get a clear outcome. Thereafter, 100 mL of 1 M NaOH were added after 15 mL of freshly made, and then 0.1 M $AgNO_3$ was added. The solution was agitated for 10 hours at 90 °C. This demonstrates the evolution of Chitosan-AgNPs [11, 12].

Synthesis of CS-AgNPs-DOX-FA conjugate

10 mL of CS-AgNPs were loaded together 1 mg of DOX, which was then mixed for 24 hours at 37 °C. The spectro-fluorometric analysis was used to measure the concentration of DOX in the supernatant working a calibration curve with excitation at 480 nm and emission at 575 nm which showed that 50 µg of DOX was added to create CS-DOX -AgNPs. Then, the solution should be stirred with 10 mg of folic acid in the dark for a day at room temperature to produce the CS-AgNPs-DOX-FA conjugate [13].

Characterization of prepared nanoparticles and conjugate

The following methods were used for the characterization: the atomic-force microscopy (AFM), field emission scanning electron microscopy (FE-SEM), and Fourier transform infrared (FT-IR) spectroscopy (FE-SEM).

The in vitro study

The MTT cytotoxicity assay

The cell viability assay, 3-[4,5-dimethylthiazol-2-yl]-2,5diphenyl tetrazolium bromide, or MTT was performed to assess the potential apoptotic-inducing activity of Dox and Chiosan-AgNPs-Doxorubicin-Folic acid conjugate. The synthesis was done at different concentration levels from Dox and Chiosan-AgNPs-Doxorubicin-Folic acid conjugate (1.5-25 µg/ml). Then, they were tested against lung cell lines A549 [14].

The tested tumorous cell lines were used to obtain 10,000 cells per well by dividing them into a 96-well plate, and each well was treated independently with varying doses of Dox and Chiosan-AgNPs-Doxorubicin-Folic acid conjugate after 24 hours. Then, the cells' vitality was determined after 72 hours of incubation, starting with medium removal followed by the addition of 28 µl MTT solution (3.27 mM) and cell incubation for 90 minutes at 37 °C. The absorption spectrum of the treated well (As) along with the control well (Ac) was measured by using a microplate reader set at 492 nm. This experiment was carried out in triplicate for every synthesized compound examined [15]. The following mathematical equation was used to obtain the growth inhibition percentage:

$$\% \text{ Growth inhibition} = (Ac-As)/Ac\times100$$

The cells were seeded inside 24-well micro-titration plates at a density of 1×10^5 cells mL^{-1} and cultured at thirty seven °C for 24 hours to observe their shape. The CS-AgNPs-DOX-FA combination and DOX were then administered to the cells for 24 hours. After applying crystal violet dye, the plates were incubated at 37 °C for 10 to 15 minutes. The color was gently removed from the stain by its rinsing with water. A digital camera mounted to the microscope was used to take pictures as the cells were observed under a 100x inverted microscope.

Apoptosis assay (AO/EtBr)

By using the AO/EtBr staining technique, the DOX and conjugate caused transience of A549 cells was evaluated. In a nutshell, cells were plated in 12-well plates for 24 hours, treated to DOX and conjugate, and then incubated for an additional 20 hours. PBS was utilized for wash the cells two times. The equal amounts to cells and two fluorescent dyes (10 µL each) were introduced for the wells. Fluorescence microscopy was then utilized to examine the cells [16].

Fluorescent labeling using FITC

By using the following method, the conjugate tagged with a fluorescent stain was created. In a nutshell, FITC was added to CS-AgNPs-DOX-FA at a condensation of 1 $mg.mL^{-1}$, and then the blend was incubated to 10 hours at room temperature. The response was stopped by using the tris buffer (pH 10). The FITC-labeled cells were centrifuged to collect them, and any unbound FITC was taken away by washing the cells 3 times in DMSO. CS-AgNPs-DOX-FA that was FITC-labeled was subsequently applied to the cells for 12 hours at 37 °C. DAPI was used to stain and mark the nuclei. By using a fluorescent microscope, pictures were taken at a 40x magnification [17].

Statistical Analysis

GraphPad Prism 6 was used to statistically evaluate the acquired data by using an unpaired t-test. The data were presented by using the average and SD of measurements made in triplicate.

Results and Discussion

Characterization of CS-AgNPs- DOX-FA

Atomic-force microscopy analysis

Figure 1 displays the distribution of the CS-AgNPs-DOX-FA conjugate and silver nanoparticles in a 3D AFM picture. Generally

speaking, the image showed which the silver NPs had a grain volume up to 7 nm and are spherical in shape.

The study of nano molecules is a significant difficult in recent nano-scale metrology. Thus, it is crucial that they are demonstrated correctly. The NPs size can be simply calculated from the AFM image by measuring the height of the nanoparticles image. A scanning probe microscope (AFM) can be used for nano molecule analysis, and it has a number of advantages over SEM/TEM for identifying different types of nano molecules. The three-dimensional data in the AFM image allows for the quantitative measurement of the nanoparticles' height [18].

Scanning electron microscope

To see how big and round the compounds were, the SEM method was used. Figures 2 and 3 indicate the findings of the SEM characterization of the created AgNPs. The SEM image showed a diameter to NPs of more than 10 nm and they were largely spherical in shape. On the other hand, the CS-Ag-NPs exhibit remarkable homogeneity in their aggregation, amorphous particles, and spherical morphologies. Their majority appear to be evenly dispersed and linked on their own [19, 20].

Fourier transforms infrared spectroscopy analysis

FT-IR was utilized to describe the produced chemical; spectra in the 4000-400 cm^{-1} wavelength region were recorded. In pure chitosan, O-H and N-H stretching bands overlap, that helps generate a peak at about 3431 cm^{-1}, that is similar to the results study in 2018 [21, 22].

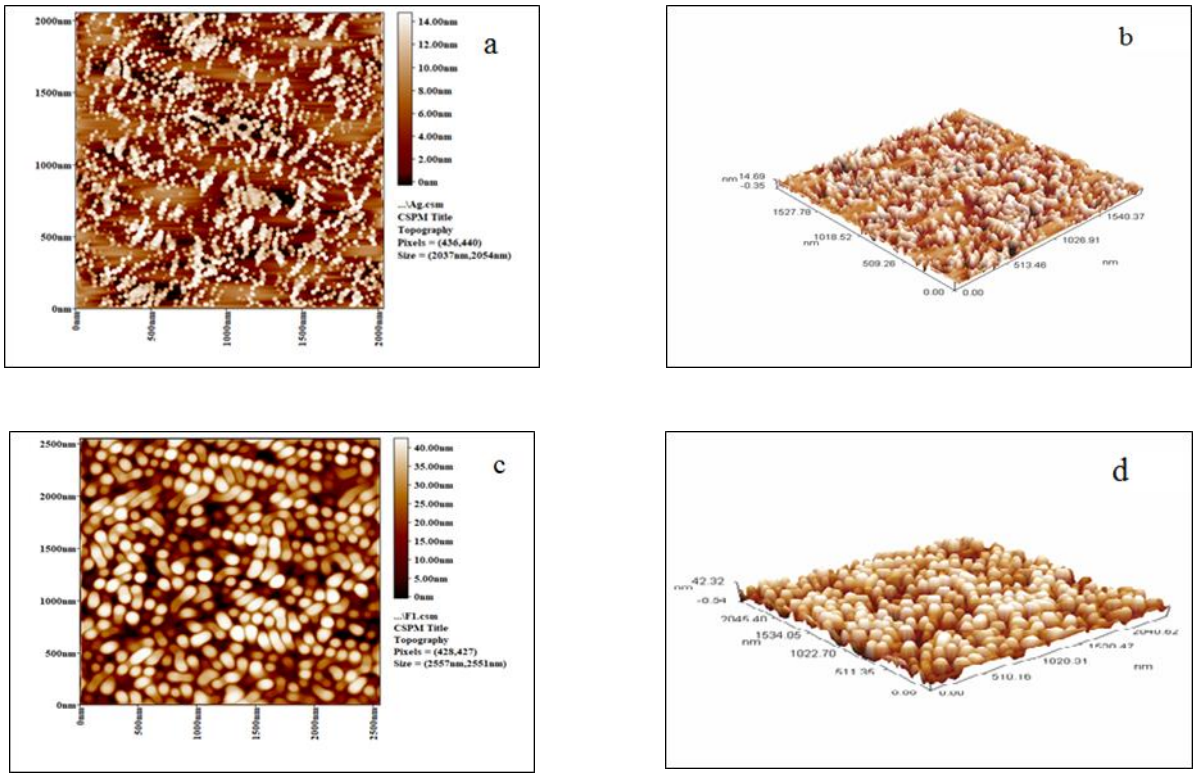

Figure 1: a,b) The atomic-force microscopy of preparation CS-AgNPs, and c,d) the atomic-force microscopy of the preparation conjugate

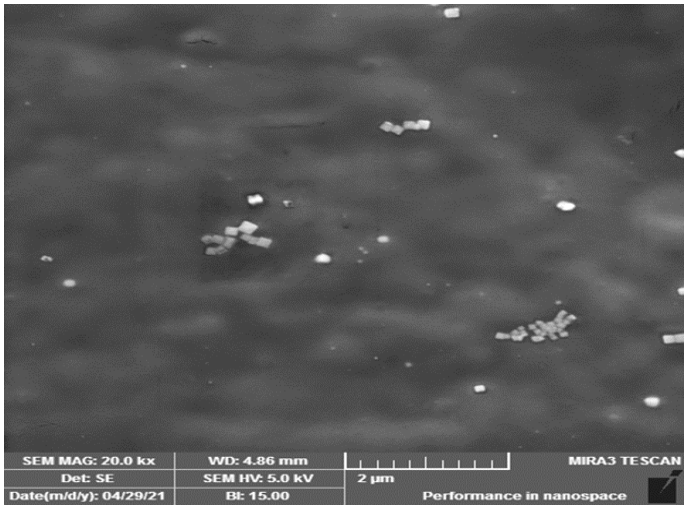

Figure 2: The SEM image of CS-AgNPs

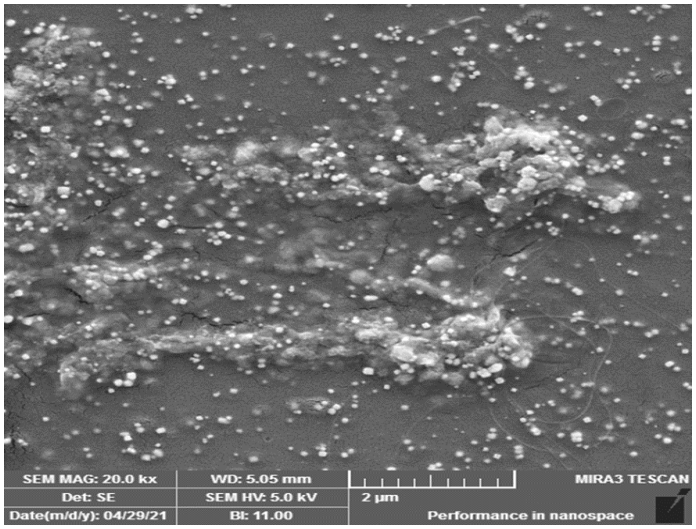

Figure 3: SEM of conjugate

The distinctive peak shifted to 3429 cm^{-1} in the Chitosan-AgNPs spectra. Pure chitosan's C-H stretching and bending peaks were found in the Chitosan-AgNPs spectra at 2918 cm^{-1} and 1427 cm^{-1}, straight. In the Chitosan-AgNPs spectra, these 2 peaks are too off-set to 2926 cm^{-1} and 1419 cm^{-1}, straight. A definite peak was created by N-H bending at 1638 cm^{-1} [23]. In the CS-AgNPs spectra, this shifted to 1625 cm^{-1}. The alcoholic C-O stretching band, ether linkage, and the C-O-C stretching band overlapped, causing a peak at 1079 cm^{-1} (Figure 4). This peak can be observed at 1081 cm^{-1} in the CS-AgNPs spectra (Figure 4). These findings are in line with the prior research that was published in 2019 [24].

To verify DOX immobilization on CS-AgNPs, the FT-IR spectra of jointly the compounds were obtained: CS-AgNPs-DOX and DOX (Figure 5). In Figure 5 [25], the DOX characteristic peaks are located at 3383 cm^{-1} and 1618 cm^{-1}. After Doxorubicin immobilization on CS-AgNPs, the FT-IR spectra of CS-AgNPs-DOX showed a frequency shift in DOX characteristic peaks to 3429 cm^{-1} and 1640 cm^{-1} and a significance decrease in strength (Figure 6). This alteration is brought about by the negative carboxylate group of DOX interacting with the positive amino group of chitosan, which covers the surface of silver nanoparticles. These results lend support to the hybridized nano-stability technology [26]. The graphic shows the FT-IR spectra of folic acid, chitosan, and FA-CS conjugates (Figure 7). Among 3600 and 3000 cm^{-1}, the stretching vibrations of (-OH) and N-H peaked in FA (Figure 8). The -CO-NH group's C=O

bond stretching vibration was observed at 1641 cm^{-1}, whereas the carboxyl group's C=O stretching vibration was observed at 1693 cm^{-1}. At 1606 cm^{-1}, the N-H vibration's bending mode was seen, while 1413 cm^{-1} was the wavelength of the phenyl structure's-OH deformation band. The signature absorption peak of the phenyl ring was seen at 1484 cm^{-1} [27]. The FT-IR spectra to CS expose the stretching vibrations of the N-H (3457 cm^{-1}) and C-H functional groups (2885 and 2847 cm^{-1}) (Figure 7). Peaks for Amide I, II, and III were 1665 cm^{-1}, 1593 cm^{-1}, and 1324 cm^{-1}, respectively. The peaks related to the symmetrical deformation of $-CH_3$ were seen at 1421 cm^{-1} and 1384 cm^{-1}, respectively, while the stretching vibrations of C-O from (C-O-C) were seen at 1153 cm^{-1} and 1088 cm^{-1} [28].

The spectra of the FA-Chitosan conjugate showed the distinctive absorption bands of both FA and CS (Figure 5). The peak caused by the deformation vibration N-H amide-II of the amine group (1598 cm^{-1}) altered of a rise frequency at 1604 cm^{-1}, it was determined that chemical interactions between FA and CS existed. The amide-III (1325 cm^{-1}) and C-O stretching vibrations (1086 cm^{-1}) peaks to CS were also shifted to 1313 and 1079 cm^{-1}, respectively.

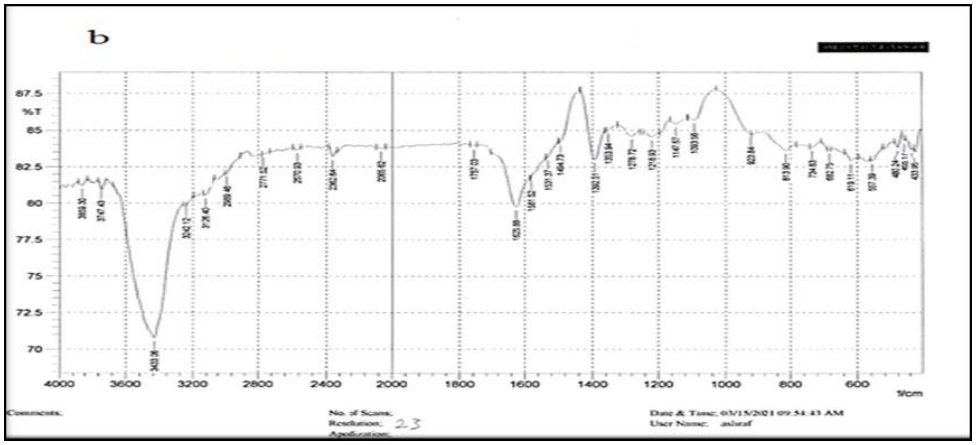

Figure 4: FT-IR to Doxorubicin AgNPs

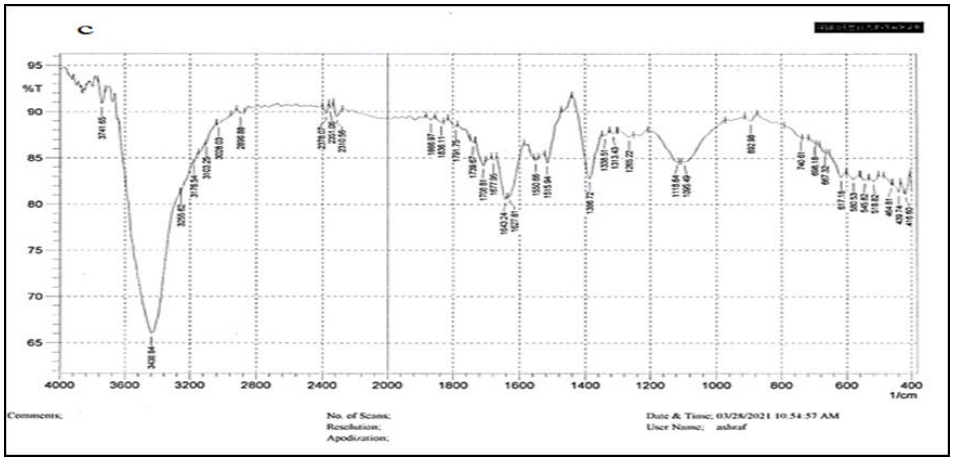

Figure 5: FT-IR to Chiosan-AgNPs-Doxorubicin-Folic acid

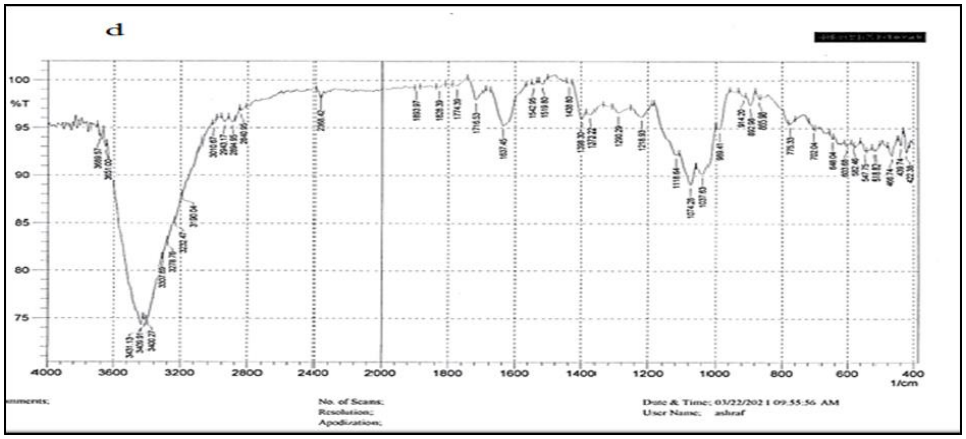

Figure 6: FT-IR to Doxorubicin

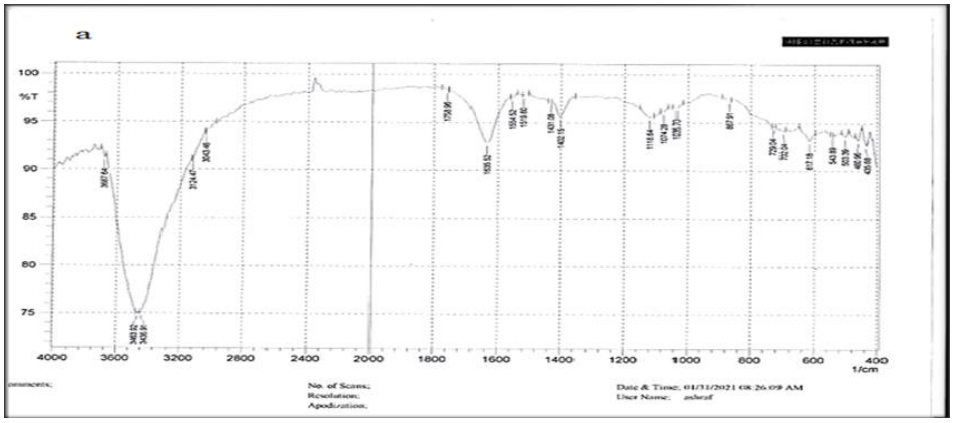

Figure 7: FT-IR to CS

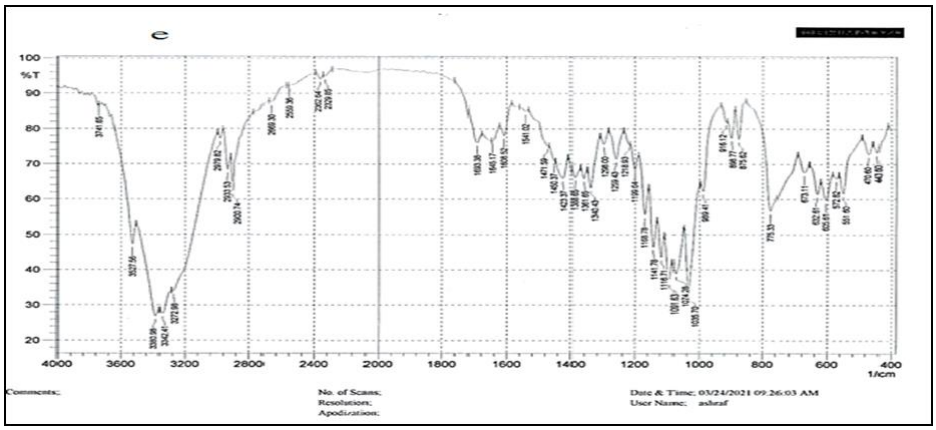

Figure 8: FT-IR to folic acid

The anticancer activity

MTT assay

For all treatments, the DOX and conjugate-treated A549 cells be visible a loss in cell viability in a dose-dependent approach over the course of 24 hours . After being exposed to the DOX and CS-AgNPs-DOX-FA conjugate for 24 hours, the growth inhibition of A549 cells varied from 6.0 ± 1.52 to 72.33 ± 1.45 and 8.00 ± 1.73 to 89.00 ± 3.21, respectively. With a maximal cytotoxicity obtained at a concentration of 25 µg/mL, CS-AgNPs-DOX-FA conjugate significantly ($P \leq 0.01$) inhibited cellular growth when compared with DOX (IC_{50} 16.77 µg/mL) and CS-AgNPs-DOX-FA conjugate (IC_{50} 10.44 µg/mL) treatments.

According to the statistics, there was no difference in the inhibition pattern of the A549 cells between DOX and the CS-AgNPs-DOX-FA conjugate (Figure 9).

After exposure to DOX at the highest concentration for 48 hours, the results revealed a substantial suppression of A549 growth. Compared for the untreated monitoring cells, there was a noticeably decreased rate of cell multiplication. A549 cell line cytotoxicity was found to be low; however, treatment with CS-AgNPs-DOX-FA combination caused the cell line to exhibit moderate cytotoxicity (Figure 10). By using an inverted phase contrast microscope, the chemicals' ability to induce apoptosis was examined through morphological changes in A549 cell line. Untreated, monitoring cells maintained their initial shape, as displayed in Figure 9. After 48 hours, cells treated with DOX and the conjugate showed the important morphological changes and substantial anti-proliferation activity.

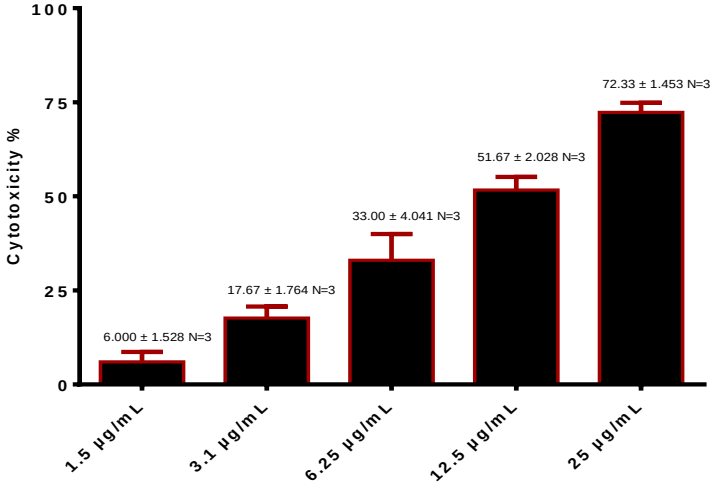

Figure 9: The cytotoxic effect of DOX in A549 cells (IC_{50}= 16.77 µg/mL)

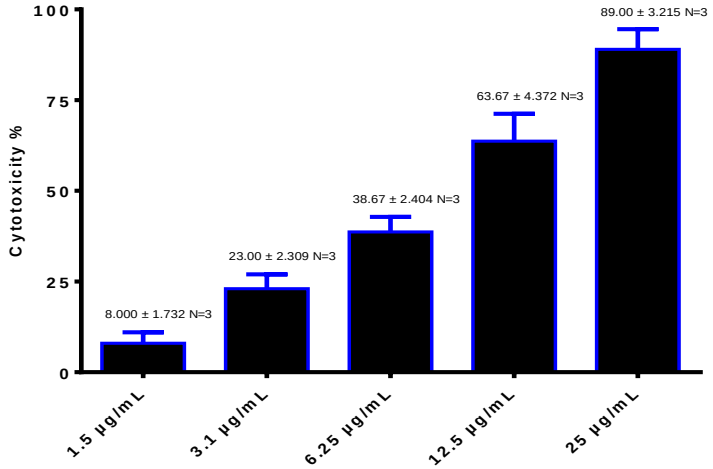

Figure 10: The cytotoxic impact of CS-AgNPs-DOX-FA conjugate in A549 cells (IC_{50}= 10.44 µg/mL)

The different expression of the multidrug resistance (MDR) gene was one factor that might have contributed to the low sensitivity of A549. A549 cells' MDR proteins contributed significantly to drug resistance and drug accommodation. In A549 cells and in all cytotoxicity studies, multidrug resistance-associated protein 1 and lung resistance-related protein were mostly expressed at high levels [29].

The AgNPs are recognized as a particularly valuable origin to potent anti-proliferative and cytotoxic factors to the specific cell lines. Because of their small size, AgNPs are easily transported into cells, where they can increase the permeability and retention (EPR) effect [30].

Nanoparticles may transport anticancer medication to particular locations by size-dependent passive targeting, which also depends on the tumor's shape and the nearby inflammatory tissues. Delivery methods for nanoparticles may take the advantage of the EPR effect, a feature of solid tumors that causes macromolecules and particulates to accumulate preferentially and to be retained in tumors for a longer period due to hyper-vascularity, defective vascular architecture, and a lack of lymphatic drainage [31].

These uniquely created nanoparticles, which combine the organic biopolymer chitosan with doxorubicin-loaded silver nanoparticles, will have a wide extent of biological applications, particularly for treatment of superficial tumors and lung cancer [32].

Cell viability and cell death were determined and measured via microscopic inspection. The DOX, CS-AgNPs-DOX-FA conjugate, and control cell line were all applied to the lung cancer cell line A549 for 24 hours. The results are demonstrated in Figure 11 indicating that after 24 hours, the control cell line did not exhibit any morphological alterations, after 24 hours of therapy with the drugs DOX and CS-AgNPs-DOX-FA combination, cancer cells' size shrank. Compared with the monitoring cells and the treated cells were fewer in number. Therefore, these outcomes revealed the efficient anticancer drug transport and DOX-loaded CS-AgNPs-DOX-FA conjugate-induced cell growth suppression.

Based on Figure 11, it is clear that as compared with free DOX, the CS-AgNPs-DOX-FA combination had a much higher cytotoxicity at little drug concentrations or at least equivalent cytotoxicity at rise drug concentrations. With longer-term cell culture, this benefit grew more importantly.

Apoptosis assay (AO/EtBr)

The dual staining test with AO/EtBr in the A549 cells lines was used to examine the cytotoxic effects of chosen doses to the synthesized DOX and conjugate in A549 cells cell lines. In contrast to DOX-treated cells and control cells, the cells were subjected to intense membrane disintegration after being treated with the CS-AgNPs-DOX-FA combination. The healthy cells displayed an intact structure without obvious apoptosis (Figure 12) and the normal green hue of the nucleus. DOX-treated cells displayed chromatin that was condensed, or fragmented, and displayed the early signs of apoptosis. Cells treated with the CS-AgNPs-DOX-FA compound, however, displayed orange nuclei and late stage apoptosis. Both living and dead cells can stain by the essential dye acridine orange. Only cells with compromised membrane integrity will be stained by ethidium bromide. Live cells will have a consistent green color. As a result of chromatin condensation and nuclear fragmentation, before time apoptotic cells will stain green and have brilliant green spots in their nuclei. In addition to incorporating ethidium bromide and staining orange, the late apoptotic cells exhibit contracted and frequently shattered nuclei as opposed to necrotic cells. The orange-stained necrotic cells lack condensed chromatin and exhibit a nuclear morphology similar to that of live cells [33]. Therefore, the changes in cell shape showed that the conjugate's method for killing cancer cells was apoptosis rather than necrosis.

The increased intracellular ROS generation may, at least in part, be to blame for the cancer-killing effects of anticancer medications, according to a prior study [34, 35]. When cancer cells were incubated with nanoparticles, there were significant effects from changes in the amounts of ROS generation on cell growth and apoptosis. However, the increased ROS levels and the resulting changed mitochondrial membrane may be responsible for phenomena including increased apoptotic morphological abnormalities and DNA damage [36].

Cellular uptake

The ability of the A 549 cell line to absorb the FITC-bound CS-AgNPs-DOX-FA combination was investigated by using fluorescent microscopy.

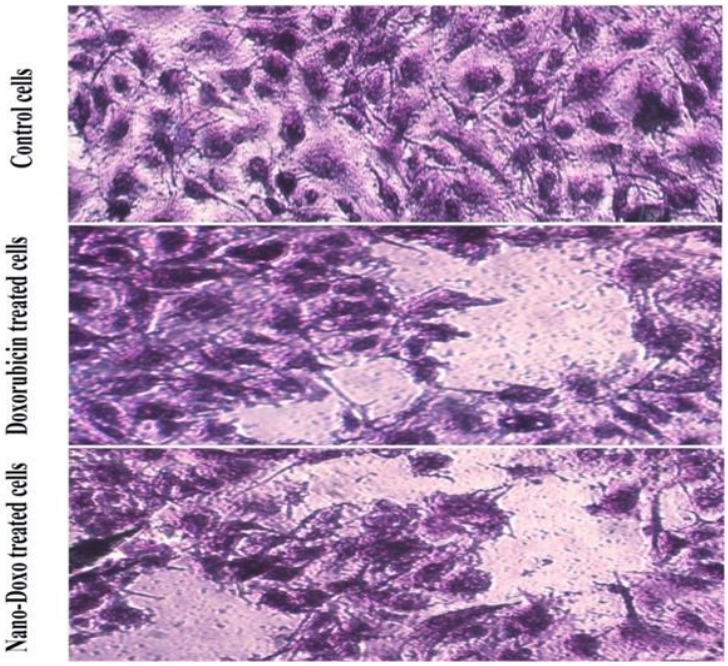

Figure 11: Morphology alteration in A549 cells when treatment with DOX and asconjugate

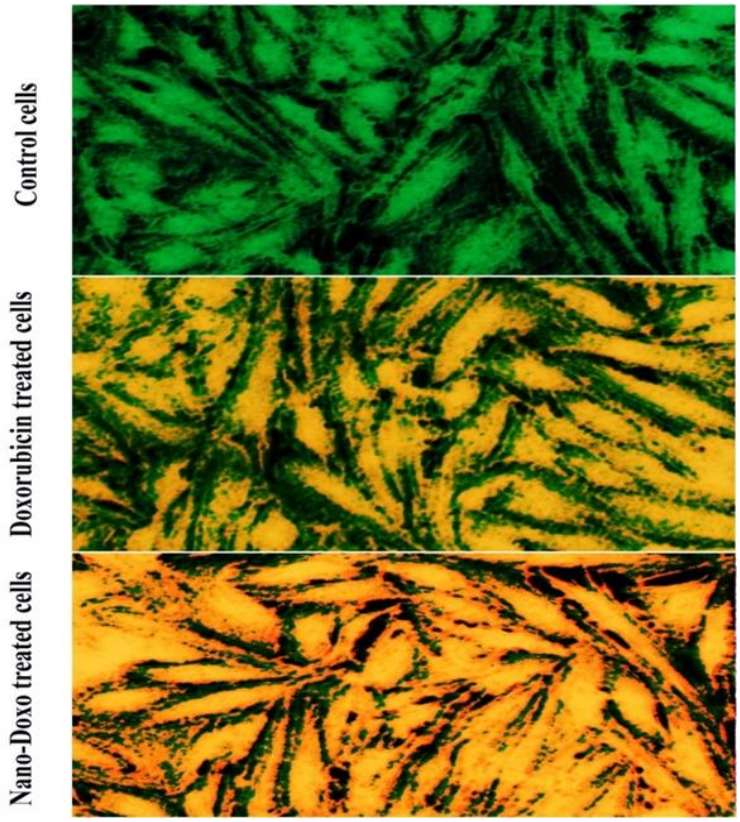

Figure 12: DOX and conjugate induce apoptosis in A549 cells

In contrast to the un-treated cells, as depicted in Figure 13, the signals with strong fluorescence that were seen in the A549 cells revealed that these chemicals were cellularly penetrated and deposited within the cytoplasm of A549 cells. Increases in fluorescence are caused by the DOX

forming π-π stacks together the aromatic groups to the DNA base pairs, which locally reduces the exposure to Doxorubicin for extrinsic quenchers. Due to its positive charge, DOX has the same propensity to join to membranes as the other positively charged molecules. Doxorubicin that was membrane-bound was confined to the cell periphery and to the membranes of vesicles [37]. This demonstrated unequivocally that the DOX came into direct touch with the DNA that was rise concentrated in the cell nucleus. This method of DOX administration is one of the drawbacks of conventional chemotherapy because it does not exhibit any specificity or selectivity for malignant cells.

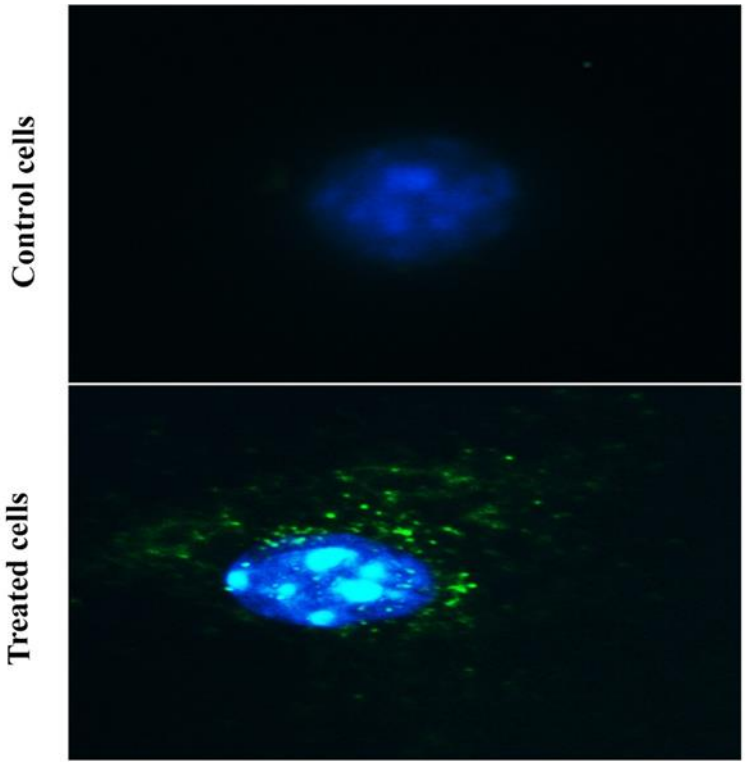

Figure 13: Cellular uptake of conjugate in A549 cells

The reduced nuclear lifetimes caused by an increase in free DOX concentration point to the beginning of fluorescence self-quenching [38]. However, it was discovered that the mechanism by which DOX exerts its deadly effects is thought to include its intercalation with DNA, which prevents the progression of the enzyme topoisomerase II before unwinding DNA for transcription. As a result, encapsulated DOX's chemotherapeutic effect is typically found to be less potent than free DOX's [39]. Numerous studies carried out by various researchers revealed variations in the mode of cellular uptake of free DOX and DOX supplied via NPs. The cellular uptake and medication delivery effectiveness are tightly connected [40]. A high drug cellular uptake can lead to a successful course of treatment. According to the reports, nanoparticles can enter cells through an energy-dependent endocytosis process [41].

Conclusion

The findings demonstrated that A549 lung cancer cells are cytotoxic to Cs-Ag NPsDOX-FA. The Cs-Ag NPs-DOX-FA MTT assay demonstrated that the harmful effect of 25 µg/mL on A549 cells is dose-dependent, and a rise in nuclear intensity, membrane permeability, and cytochrome were observed. Cell viability also declined, and the potential of the mitochondrial membrane changed. The fact that the release of DOX was delayed shows that nanoparticles in drug carriers may be used to reduce the exposure of healthy tissues however boosting the accumulation to therapeutic medicine in the tumor site.

Acknowledgements

The authors thank the Iraqi Center for Cancer and Medical Genetic Research for their help in the *in vitro* study spatially Dr. Majid S. Jabir.

Disclosure Statement

No potential conflict of interest was reported by the authors.

Funding

This research did not receive any specific grant from funding agencies in the public, commercial, or not-for-profit sectors.

Authors' contributions

All authors contributed to data analysis, drafting, and revising of the paper and agreed to be responsible for all the aspects of this work.

References

[1]. Weiderpass E., Hashim D., Labrèche F., Malignant tumors of the female reproductive system, In *Occupational Cancers*, 2020, (439-453, Springer, Cham. [Crossref], [Google Scholar], [Publisher]

[2]. Kiriiri G.K., Njogu P.M., Mwangi A.N., Exploring different approaches to improve the success of drug discovery and development projects: a review, *Future Journal of Pharmaceutical Sciences*, 2020, **6**:27 [Crossref], [Google Scholar], [Publisher]

[3]. Lin A., Giuliano C.J., Palladino A., John K.M., Abramowicz C., Yuan M.L., ... Sheltzer J.M., Off-target toxicity is a common mechanism of action of cancer drugs undergoing clinical trials, *Science translational medicine*, 2019, **11**:8412 [Crossref], [Google Scholar], [Publisher]

[4]. Bale A.S., Khatokar J.A., Singh S., Bharath G., Mohan M.K., Reddy S.V., Satheesha T.Y., Huddar S.A., Nanosciences fostering cross domain engineering applications, *Materials Today: Proceedings*, 2021, **43**:3428 [Crossref], [Google Scholar], [Publisher]

[5]. Kolahalam L.A., Viswanath I.K., Diwakar B.S., Govindh B., Reddy V., Murthy Y.L.N., Review on nanomaterials: Synthesis and applications, *Materials Today: Proceedings*, 2019, **18**:2182 [Crossref], [Google Scholar], [Publisher]

[6]. Ashindortiang O.I., Anyama C.A., Ayi A.A., Phytosynthesis, Characterization and Antimicrobial Studies of Silver Nanoparticles Using Aqueous Extracts of OlaxSubscorpioidea, 2022, **5**:215 [Crossref], [Google Scholar], [Publisher]

[7]. Tran S., DeGiovanni P.J., Piel B., Rai P., Cancer nanomedicine: a review of recent success in drug delivery. Clinical and translational medicine, 2017, **6**:e44 [Crossref], [Google Scholar], [Publisher]

[8]. Aftab S., Shah A., Nadhman A., Kurbanoglu S., Ozkan S.A., Dionysiou D.D., Shukla S.S., Aminabhavi T.M., Nanomedicine: An effective tool in cancer therapy, *International journal of pharmaceutics*, 2018, **540**:132 [Crossref], [Google Scholar], [Publisher]

[9]. Bobo D., Robinson K.J., Islam J., Thurecht K.J., Corrie S.R., Nanoparticle-based medicines: a review of FDA-approved materials and clinical trials to date, *Pharmaceutical research*, 2016, **33**:2373 [Crossref], [Google Scholar], [Publisher]

[10]. Paradise J., Regulating nanomedicine at the food and drug administration, *AMA Journal of Ethics*, 2019, **21**:347 [Crossref], [Google Scholar], [Publisher]

[11]. Sanpui P., Chattopadhyay A., Ghosh S.S., Induction of apoptosis in cancer cells at low silver nanoparticle concentrations using chitosan nanocarrier, *ACS applied materials & interfaces*, 2011, **3**:218 [Crossref], [Google Scholar], [Publisher]

[12]. Mohammadi R., Sonocatalytic degradation of methyl red by sonochemically synthesized TiO2-SiO2/chitosan nanocomposite, *Quarterly Journal of Iranian Chemical Communication*, 2020, **8**:145 [Google Scholar]

[13]. Kareem S.H., Naji A.M., Taqi Z.J., Jabir M.S., Polyvinylpyrrolidone loaded-MnZnFe2O4 magnetic nanocomposites induce apoptosis in cancer cells through mitochondrial damage and P53 pathway, *Journal of Inorganic and Organometallic Polymers and Materials*, 2020, **30**:5009 [Crossref], [Google Scholar], [Publisher]

[14]. Alshibl H.M., Al-Abdullah E.S., Haiba M.E., Alkahtani H.M., Awad G.E., Mahmoud A.H.,

Ibrahim B.M.M., Bari A., Villinger A., Synthesis and evaluation of new coumarin derivatives as antioxidant, antimicrobial, and anti-inflammatory agents, *Molecules*, 2020, **25**:3251 [Crossref], [Google Scholar], [Publisher]

[15]. Mustafa Y.F., Riyadh Khalil R., Tareq Mohammed E., Bashir M.K., Khudhayer Oglah M., Effects of structural manipulation on the bioactivity of some coumarin-based products, *Archives of Razi Institute*, 2021, **76**:1297 [Crossref], [Google Scholar], [Publisher]

[16]. Cheng S., Qian F., Huang Q., Wei L., Fu Y., Du Y., HOXA4, down-regulated in lung cancer, inhibits the growth, motility and invasion of lung cancer cells, *Cell death & disease*, 2018, **9**:465 [Crossref], [Google Scholar], [Publisher]

[17]. Barbero N., Barolo C., Viscardi G., Bovine serum albumin bioconjugation with FITC, *World Journal of Chemical Education*, 2016, **4**:80[Crossref], [Google Scholar], [Publisher]

[18]. Pavliček N., Gross L., Generation, manipulation and characterization of molecules by atomic force microscopy, *Nature Reviews Chemistry*, 2017, **1**:0005 [Crossref], [Google Scholar], [Publisher]

[19]. Gharibshahi L., Saion E., Gharibshahi E., Shaari A.H., Matori K.A., Structural and optical properties of Ag nanoparticles synthesized by thermal treatment method, *Materials*, 2017, **10**:402 [Crossref], [Google Scholar], [Publisher]

[20]. Dagne T., synthesis and characterization of low cost activated carbon prepared from water hyacinth stem by phospheric for removal of chromium ion in aqueous solution, equilibrium and kinetic study, (Doctoral dissertation), 2021 [Google Scholar], [Publisher]

[21]. Ibrahim H.M., Farid O.A., Samir A., Mosaad R.M., Preparation of chitosan antioxidant nanoparticles as drug delivery system for enhancing of anti-cancer drug, n *Key Engineering Materials*, Trans Tech Publications Ltd, 2018, **759**:92 [Crossref], [Google Scholar], [Publisher]

[22]. Lai H., Liu Y., Huang G., Chen Y., Song Y., Ma Y., Yue P., Fabrication and antibacterial evaluation of peppermint oil-loaded composite microcapsules by chitosan-decorated silica nanoparticles stabilized Pickering emulsion templating, *International Journal of Biological Macromolecules*, 2021, **183**:2314 [Crossref], [Google Scholar], [Publisher]

[23]. Han D., Yan L., Chen W., Li W., Preparation of chitosan/graphene oxide composite film with enhanced mechanical strength in the wet state, *Carbohydrate Polymers*, 2011, **83**:653 [Crossref], [Google Scholar], [Publisher]

[24]. Hajji S., Khedir S.B., Hamza-Mnif I., Hamdi M., Jedidi I., Kallel R., Sami B., Nasri M., Biomedical potential of chitosan-silver nanoparticles with special reference to antioxidant, antibacterial, hemolytic and in vivo cutaneous wound healing effects, *Biochimica et BiophysicaActa (BBA)-General Subjects*, 2019, **1863**:241 [Crossref], [Google Scholar], [Publisher]

[25]. Laghrib F., Ajermoun N., Bakasse M., Lahrich S., El Mhammedi M.A., Synthesis of silver nanoparticles assisted by chitosan and its application to catalyze the reduction of 4-nitroaniline, *International journal of biological macromolecules*, 2019, **135**:752 [Crossref], [Google Scholar], [Publisher]

[26]. Victor S.P., Paul W., Jayabalan M., Sharma C.P., Supramolecular hydroxyapatite complexes as theranostic near-infrared luminescent drug carriers, *CrystEngComm*, 2014, **16**:9033 [Crossref], [Google Scholar], [Publisher]

[27]. Ali S.W., Rajendran S., Joshi M., Synthesis and characterization of chitosan and silver loaded chitosan nanoparticles for bioactive polyester, *Carbohydrate Polymers*, 2011, **83**:438 [Crossref], [Google Scholar], [Publisher]

[28]. Seifirad S., Karami H., Shahsavari S., Mirabasi F., Dorkoosh F., Design and characterization of mesalamine loaded nanoparticles for controlled delivery system, *Nanomedicine Research Journal*, 2016, **1**:97 [Crossref], [Google Scholar], [Publisher]

[29]. Schonfeld S.J., Curtis R.E., Anderson W.F., Berrington de González A., The risk of a second primary lung cancer after a first invasive breast cancer according to estrogen receptor status, *Cancer Causes & Control*, 2012, **23**:1721 [Crossref], [Google Scholar], [Publisher]

[30]. Gliga A.R., Skoglund S., OdnevallWallinder I., Fadeel B., Karlsson H.L., Size-dependent cytotoxicity of silver nanoparticles in human lung cells: the role of cellular uptake, agglomeration

and Ag release, *Particle and fibre toxicology*, 2014, **11**:11 [Crossref], [Google Scholar], [Publisher]
[31]. Aghebati-Maleki A., Dolati S., Ahmadi M., Baghbanzhadeh A., Asadi M., Fotouhi A., Yousefi M., Aghebati-Maleki L., Nanoparticles and cancer therapy: Perspectives for application of nanoparticles in the treatment of cancers, *Journal of cellular physiology*, 2020, **235**:1962 [Crossref], [Google Scholar], [Publisher]
[32]. Lohiya G., Katti D.S., Carboxylated chitosan-mediated improved efficacy of mesoporous silica nanoparticle-based targeted drug delivery system for breast cancer therapy, *Carbohydrate Polymers*, 2022, **277**:118822 [Crossref], [Google Scholar], [Publisher]
[33]. Wu H., Chen L., Zhu F., Han X., Sun L., Chen K., The cytotoxicity effect of resveratrol: cell cycle arrest and induced apoptosis of breast cancer 4T1 cells, *Toxins*, 2019, **11**:731 [Crossref], [Google Scholar], [Publisher]
[34]. Hayes J.D., Dinkova-Kostova A.T., Tew K.D., Oxidative stress in cancer, *Cancer cell*, 2020, **38**:167 [Crossref], [Google Scholar]
[35]. Jasim S.F., Mustafa Y.F., New fused-coumarin composites: synthesis, anticancer and antioxidant potentials evaluation, *Eurasian Chemical Communications*, 2022, **4**:607 [Crossref], [Google Scholar], [Publisher]
[36]. Dharmaraja A.T., Role of reactive oxygen species (ROS) in therapeutics and drug resistance in cancer and bacteria. *Journal of Medicinal Chemistry*, 2017, **60**:3221 [Crossref], [Google Scholar], [Publisher]
[37]. Dai X., Yue Z., Eccleston M.E., Swartling J., Slater N.K.H., Kaminski C.F., Fluorescence intensity and lifetime imaging of free and micellar-encapsulated doxorubicin in living cells. In Nanomedicine in Cancer, *Jenny Stanford Publishing*, 2017, **4**:49 [Crossref], [Google Scholar], [Publisher]
[38]. Manaspon C., Viravaidya-Pasuwat K., Pimpha N., Preparation of folate-conjugated pluronic F127/chitosan core-shell nanoparticles encapsulating doxorubicin for breast cancer treatment, *Journal of Nanomaterials*, 2012, **2012**:593878 [Crossref], [Google Scholar], [Publisher]
[39]. Ramalingam V., Varunkumar K., Ravikumar V., Rajaram R., Target delivery of doxorubicin tethered with PVP stabilized gold nanoparticles for effective treatment of lung cancer, *Scientific reports*, 2018, **8**:3815 [Crossref], [Google Scholar], [Publisher]
[40]. Su W.P., Cheng F.Y., Shieh D.B., Yeh C.S., Su W.C., PLGA nanoparticles codeliver paclitaxel and Stat3 siRNA to overcome cellular resistance in lung cancer cells, *International journal of nanomedicine*, 2012, **7**:4269. [Crossref], [Google Scholar], [Publisher]
[41]. Benfer M., Kissel T., Cellular uptake mechanism and knockdown activity of siRNA-loaded biodegradable DEAPA-PVA-g-PLGA nanoparticles, *European Journal of Pharmaceutics and Biopharmaceutics*, 2012, **80**:247 [Crossref], [Google Scholar], [Publisher]

HOW TO CITE THIS ARTICLE
Manar S. Jabar, Shatha Abdul Wadood Al- Shammaree. Cytotoxicity and Anticancer Effect of Chitosan-Ag NPs-Doxorubicin-Folic Acid Conjugate on Lungs Cell Line. *Chem. Methodol.*, 2023, 7(1) 1-14
https://doi.org/10.22034/CHEMM.2023.359769.1604
URL: http://www.chemmethod.com/article_158118.html